

http://pubs.acs.org/journal/aesccq Article

Evolution of Oxygen Isotopologues in Phosphate and Pyrophosphate during Enzyme-Catalyzed Isotopic Exchange Reactions

Spencer R. Moller, Yuriy Sakhno, Ludmilla Aristilde, Ruth E. Blake, and Deb P. Jaisi*



Cite This: https://doi.org/10.1021/acsearthspacechem.2c00050



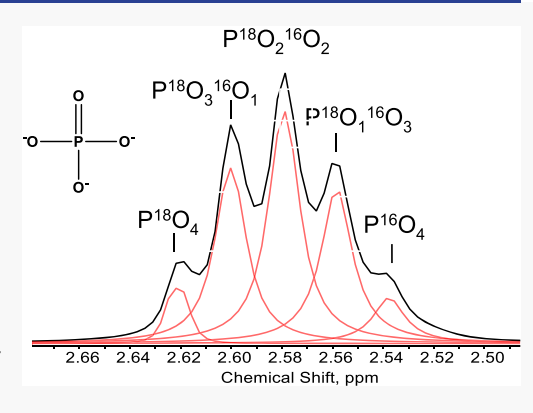
ACCESS

III Metrics & More

Article Recommendations

s Supporting Information

ABSTRACT: Inorganic pyrophosphatase (PPase) is an enzyme that catalyzes the hydrolysis of the phosphoanhydride bond in pyrophosphate (PP_i) to release inorganic phosphate (P_i) and simultaneously exchange oxygen isotopes between P_i and water. Here, we quantified the exchange kinetics of oxygen isotopes between five P_i isotopologues (P¹⁸O₄, P¹⁸O₃¹⁶O, P¹⁸O₂¹⁶O₂, P¹⁸O¹⁶O₃, and P¹⁶O₄) and water using Raman spectroscopy and ³¹P nuclear magnetic resonance (NMR) during the PPase-catalyzed ¹⁸O⁻¹⁶O isotope exchange reaction in P_i water and PP_i-water systems. At a high PP_i concentration (300 mM), hydrolysis of PP_i by PPase was predominant, and only a small fraction of PP_i (\ll 1%) took part in the reversible hydrolysis—condensation reaction (PP_i \leftrightarrow P_i), leading to the oxygen isotope exchange between P_i and water. We demonstrated that Raman and NMR methods can be equally applied for monitoring the kinetics of the oxygen exchange between the P_i isotopologue and water. It was found that the isotope exchange determined by the spectroscopic methods was detectable as



low as 0.2% ¹⁸O abundance, but the reliability below 1% was much lower. Given that high P concentrations (≥ 1 mM) are required in these methods, environmental application of these methods is limited to rare high P conditions in engineered and agricultural environments.

KEYWORDS: pyrophosphatase (PPase), isotope kinetics, ¹⁸O-¹⁶O isotope exchange, Raman spectroscopy, NMR spectroscopy

■ INTRODUCTION

Biological reactions mediated by phosphatase-type enzymes are an essential component of the phosphorus (P) cycle in living organisms that play a critical role in the production of bioavailable P in natural environments. The phosphate oxygen isotope effect in inorganic P (PO₄, referred to as P_i hereafter) provides useful information to identify the extent of P cycling in various microbially mediated reactions to discriminate from abiotic reactions.¹⁻³ This distinction is possible because oxygen isotope exchange occurs in the presence of different phosphatase enzymes, which often have specific yet distinct isotope effects.⁴ Phosphoryl transfer enzymes are one of the largest classes of enzymes,5 which include inorganic pyrophosphatase (PPase), a ubiquitous intracellular enzyme essential to P metabolism.^{6,7} The primary function of PPase is to catalyze the condensation of P_i to pyrophosphate (PP_i) as well as to hydrolyze PP, to produce P, leading to rapid reversible (equilibrium) oxygen isotope exchange between P_i and water. 8,9 PP,, the shortest P chain containing two P atoms linked by a high-energy phosphoanhydride bond, is the byproduct of nearly 200 cellular biosynthetic reactions wherein ATP is converted to AMP.¹⁰ Thus, in these metabolic reactions, PP_i acts as the energy coin in living organisms.¹ Furthermore, hydrolysis of PP, represents an intrinsic and

critical step of DNA synthesis.¹¹ In contrast to PPase, all other known phosphoesterase enzymes catalyze the hydrolysis of ester bonds in organic P compounds through a unidirectional (disequilibrium) reaction.¹² Therefore, both equilibrium and disequilibrium oxygen isotope signatures are proxies for assessing the presence of biological activity in various ecosystems.

Reliable interpretation of oxygen isotope variations for P_i in different forms (such as a dissolved ion, sorbed ion, or incorporated within the mineral structure) for both natural and engineered environments requires to account for the kinetics of the oxygen isotope exchange between dissolved P_i species and water. The conventional assumption is that the oxygen isotopes of phosphate minerals precipitated from an aqueous solution would record the corresponding isotopes of dissolved oxyanion species with only a minor fractionation (<1‰). 13,14

Received: February 18, 2022 Revised: April 23, 2022 Accepted: April 26, 2022



Furthermore, the dissolved phosphate is assumed to be in equilibrium with coexisting water. However, the validations of this assumption are restricted in rock records because of the inability to collect coexisting phases (e.g., water and Pi) in which equilibria occurred before precipitation of minerals. For many soils and sediments where coexisting phases are available, relatively more cases of the nonequilibrium isotopes are reported. 15-17 This means that the validations are limited to controlled laboratory studies. Thermodynamic equilibrium isotope values are relatively straightforward to calculate because they are based on well-known principles of statistical thermodynamics and quantum mechanics. 18 However, fundamental knowledge on the kinetics of the oxygen isotope exchange is relatively limited, particularly for P_i compared to other oxyanions such as carbonates, sulfates, and silicates. 19-22 Thus, studies of real-time and high-resolution substitutions in isotopologues are rare. 23-25 The available theories on isotope substitution²⁶ have not yet been tested for a phosphatic system.

Isotope ratio mass spectrometry (IRMS) is a commonly used and reliable technique for measuring isotopes of light elements, with analytical precision generally at $\leq 0.1\%$ and with reproducibility typically better than $\pm 0.3\%$ for phosphate oxygen isotopes.²⁷ However, the kinetics of specific isotopologues may not be distinguishable by IRMS because this method is destructive and requires the breaking of molecules to extract atoms for 'bulk' isotope measurement. Therefore, IRMS methods do not permit high-resolution temporal analyses of any isotopes because of the unusually long time needed to preprocess and purify the analyte. The multistep purification process may also introduce processing-related artifacts and impact the final isotope value. Given that enzymecatalyzed isotope exchange reactions are too fast for the IRMSbased methods, an in-depth understanding of the kinetics of isotopologue exchange demands the use of techniques that are nondestructive and, more importantly, capable of detecting isotope exchanges in real time. The objective of this research was to quantify the kinetics of isotope exchange between five isotopologues of P_i ($P^{18}O_4$, $P^{18}O_3^{16}O_2$, $P^{18}O_2^{16}O_2$, $P^{18}O^{16}O_3$, and P¹⁶O₄) during enzyme-catalyzed ¹⁸O-¹⁶O isotope exchange in Pi-water and PPi-water systems. Here, we utilized Raman and nuclear magnetic resonance (NMR) spectroscopy methods to detect the changes in oxygen isotopes between P_i isotopologues and water in real time during the PPasecatalyzed equilibration reactions.

MATERIALS AND METHODS

Reagents and Enzymes. Oxygen isotope-labeled compounds, potassium dihydrogen phosphate ($^{18}O_4$, 99.7%) and water (^{18}O , 10 and 99%), were purchased from Cambridge Isotope Laboratories, Inc. Inorganic pyrophosphatase, from *Escherichia coli* (EC 3.6.1.1), was purchased from Sigma-Aldrich as a lyophilized powder and stored at -20 °C. After reconstitution, the enzyme was used for the experiment or stored at -20 °C for future use. Reagent-grade (ACS) sodium pyrophosphate tetrabasic decahydrate, magnesium chloride hexahydrate, and sodium hydroxide were purchased from Acros Organics.

Experimental Setup. To identify the spectral characteristics of isotopically labeled and nonlabeled P_i and PP_i [^{18}O -enriched potassium dihydrogen phosphate ($^{18}O_4$, 99.7%), potassium dihydrogen phosphate ($^{16}O_4 > 99\%$), and sodium pyrophosphate ($^{16}O_4 > 99\%$)], each of them were individually

dissolved in sterile deionized water, kept at pH 9.0 using 0.1 or 0.5M NaOH, and analyzed by Raman and NMR spectroscopy methods. All reaction solutions were prepared in deionized water that was autoclaved or filter-sterilized using a 0.2 μ m syringe filter in a Herasafe (Thermo Scientific) biosafety cabinet. Based on a series of Raman measurements, discernible spectra were apparent at about 0.5 mM for P_i and PP_i , but a higher concentration is needed for better confidence on spectral resolution. Several pilot experiments were performed with a range of enzyme and metal cofactor concentrations to establish an optimal experimental condition for enzyme activity for accurate measurements of $^{18}O^{-16}O$ isotope exchange within the resolution of the analytical time frame of Raman and NMR spectroscopy.

In the first set of experiments, isotopically labeled P_i was used to monitor the evolution of the isotopologues of P_i and to quantify the isotope exchange between P_i and water. Based on the preliminary results, detailed enzyme-catalyzed oxygen isotope exchange reactions between P_i and water were chosen as follows: 300 mM $^{18}\text{O-enriched}$ phosphate, 5 mM magnesium as a cofactor, and 50 U (total activity) of PPase from Escherichia coli(EC 3.6.1.1). The pH of the reaction solution (5 mL) was kept constant at 9.0 (±0.1) using NaOH before the addition of PPase for the optimal enzyme activity specified by the manufacturer. We chose not to use an organic buffer to avoid any background fluorescence effect during spectroscopic measurements.

The second set of experiments was performed to study enzyme-catalyzed hydrolysis of PP_i and subsequent oxygen isotope exchange between P_i and water. The reaction mixture consisted of 100 mM PP_i prepared in labeled water (¹⁸O, 99%), 50 mM magnesium (as $MgCl_2$) as a cofactor, and 50 U of PPase from *Escherichia coli* (EC 3.6.1.1). The enzyme and metal cofactors were prepared separately in ¹⁸O-labeled water (¹⁸O = 10%). The pH of the substrate and cofactor solutions was kept constant at 9.0 (\pm 0.1) using NaOH before the addition of PPase.

Two separate control experiments were performed to (i) test the stability of the substrates and the occurrence of any abiotic oxygen isotope exchange and (ii) determine the effects of the cofactor addition in experiments on the efficiency of enzymatic activity. In the first experiment, 300 mM $P_2^{18}O_4$ and 100 mM $P_2^{16}O_7$ were prepared separately without PPase but with 5 mM and 50 mM magnesium as a cofactor, respectively, at pH 9.0 in $H_2^{16}O$ (unlabeled deionized water). The second set of experiment was identical to the first, but with 50 U of PPase enzyme and without the presence of a cofactor. All sets of experiments were conducted in triplicate at room temperature (20 °C) under a Herasafe (Thermo Scientific) biosafety cabinet and monitored for up to 500 days.

Analytical Methods of Characterization. Analysis of the oxygen isotope exchange using Raman spectroscopy is feasible because the substitution of 16 O in P_i by 18 O in water causes a measurable shift of the fully symmetric stretching mode of the PO_4^{3-} ion. In this study, Raman spectroscopy measurements were carried out in a quartz-glass cuvette using a Kaiser RXN spectrometer equipped with a laser (785 nm, 97 mW) and a HoloSpec f/1.8i VPT detector. All spectra were collected in low lambda mode at 1 s of laser exposure with 60 scans per spectra collection. The spectra were collected over a series of subsamples collected during the span of isotope exchange reactions. Data were processed and analyzed using the GRAMS/AI program. To accurately quantify the different

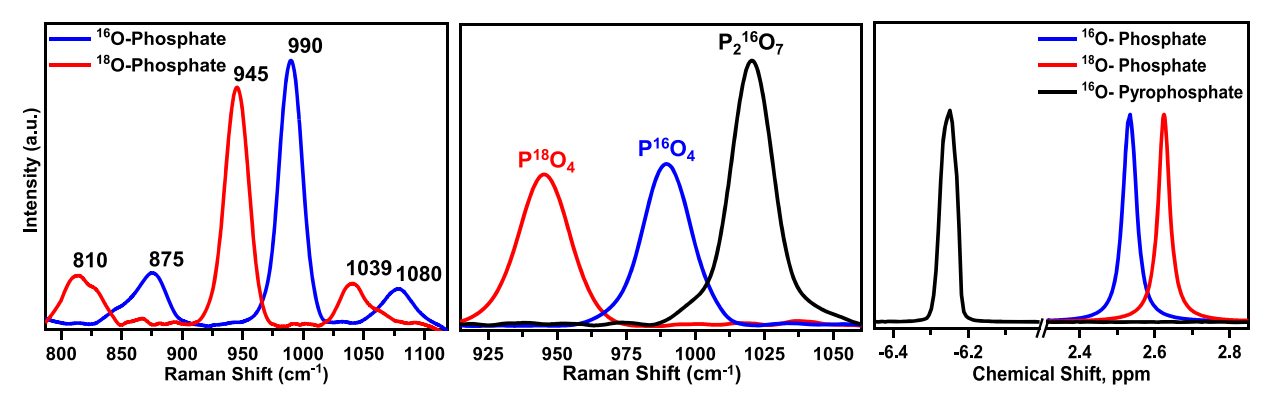


Figure 1. (a) Spectral separation 16 O and 18 O in P_i and PP_i . (a) Raman shifts of P^{16} O₄ (blue) and P^{18} O₄ (red), (b) Raman shifts of P_2^{16} O₇ (black), P^{16} O₄ (blue), and P^{18} O₄ (red), and (c) 31 P NMR spectra of P^{16} O₄, P^{18} O₄, and P_2^{16} O₇. The concentrations used were 100 mM for PP_i and 300 mM for P_i . The antisymmetric stretching of the Raman band of P^{16} O₄ at 1039.2 cm⁻¹ is not visible in these spectra.

isotopologues, curve fitting was performed using the OPUS base package applying Gaussian/Lorentzian functions.

The 16O and 18O isotopes are not NMR-active nuclei because of their even mass and even charge, which results in zero nuclear spin. However, ¹⁸O ↔ ¹⁶O isotopic substitution imparts small chemical shifts in the ³¹P nucleus. Therefore, ³¹P NMR can be used to study isotope exchange caused by enzymatic reactions, which were first confirmed in adenosine phosphates.²⁸ In this study, the active resonance nuclei (P) were analyzed by conventional ³¹P NMR spectroscopy in an AVIII 600 MHz Bruker spectrometer equipped with a 5 mm Bruker SMART probe. 10% D₂O was used as the reference lock, and 2 mM EDTA was added as a chelating agent in all samples before measurement. The ³¹P NMR is highly sensitive to pH changes because the density of the electron cloud surrounding the ³¹P nucleus decreases with increasing acidic strength of the Brønsted acid site, which results in the 31P resonance shifting downfield direction (i.e., higher chemical shift). To avoid any changes in the chemical shift as well as the potential impact on the kinetics of oxygen isotope exchange, pH was adjusted to starting pH 9.0 (±0.1) during all spectral data collections.

The NMR acquisition parameters were as follows: 32 composite-pulse decoupled scans, four dummy scans, 2 s relaxation delay, 0.67 s acquisition time, FID size 32,768, apodized with 1 Hz line broadening, and center frequency of 0 ppm at 243.01 MHz. A set of analyses was performed in real time in the NMR under identical experimental conditions. Data were processed in the OPUS base package, similar to Raman data, for quantitative analyses of isotopologues. To accurately account for the small contribution of ¹⁸O and ¹⁶O at the early and late phases of the experiments, respectively, curve fitting was carefully reviewed by zooming in the respective regions and the best fit was adopted using the OPUS program.

Theoretical Raman Shift Calculations. Raman spectroscopy allows for the monitoring of isotope exchange reactions because the substitution of 18 O in dissolved phosphate by 16 O from water causes a blue shift. The integrated intensity of a fundamental Raman band of a molecular species depends on the (i) concentration of Raman-active species, (ii) Raman beam cross-section which determines the scattering efficiency, (iii) self-absorption, (iv) depolarization ratio of the species present in the solution, (v) excitation frequency and intensity, and (vi) the response function of the instrument used. ¹⁹ It means for the same scattering efficiency, the relative contribution of symmetric stretching ($\nu_{\rm sym}$) in the range of

925–1025 cm⁻¹ from five isotopologues can be determined by integrating band intensities. The isotopic substitutions and corresponding Raman shifts can then be attributed to the mass effect during oxygen isotope exchange.²⁹

For each P_i isotopologue, the Raman shift can be theoretically calculated by treating the P-O stretching motion of Raman scattering as a harmonic oscillator. If substitution by atoms of different valency occurs, such as K^+ replaced by Mg^{2+} , it influences the force constant and causes a slight variation in Raman shifts. The calculated Raman shifts (v_i) are determined using the measured peak positions of pure $P^{16}O_4$ (v_0), the number of $P^{18}O_4$ atoms in P_i (1, 2, 3, or 4), and the masses of $P^{16}O_4$ and $P^{18}O_4$ isotopes ($P^{18}O_4$ and $P^{18}O_4$):

$$\nu_i = \nu_0 \sqrt{\frac{i \cdot m_{16} + (4 - i) \cdot m_{18}}{4 \cdot m_{18}}}$$

The theoretical Raman shifts (cm⁻¹) of enriched PO₄ isotopologues ($P^{16}O_3^{18}O$, $P^{16}O_2^{18}O_2$, $P^{16}O^{18}O_3$, and $P^{18}O_4$) and most abundant isotopologue ($P^{16}O_4$) are calculated using the above equation, and the results are reported in Table S1. The frequencies of experimental P_i and its isotopologues are included in Table S2 as observed by the Raman spectral changes during the oxygen isotope exchange between P_i and water.

Spectroscopic Data Analysis. Raman intensity is disproportionate to the relative concentrations of the Ramanactive molecules P18O4 and P16O4 because of the difference in their molar extinction coefficients. This means that P18O4 and P¹⁶O₄ of the same concentrations do not have the same band intensity but rather follow the isotope sum rule that A_i/ν_i is a constant, where A is the integrated intensity for the individual band and ν is the Raman shift. Thus, each signal intensity is proportional to the concentration, which facilitates calculating the extent of isotope exchange. Unlike NMR, slight variation of pH does not affect the integrated intensity of Raman peaks.³⁰ On the other hand, ³¹P NMR intensity is proportional to the relative concentrations of P18O4 and $P^{16}O_{4}$, which means that the integrated intensity can be directly compared to calculate the concentrations of corresponding isotopologues. Here, the relative contribution of each isotopologue was computed by integration as fractions of the total intensity under Gaussian curve. Each band was not corrected to the difference in intensities $\nu_{\rm sym}$ $P^{18}{\rm O}/P^{16}{\rm O}$ because of its irrelevance for quantification. A separate calculation was made in which measured intensity of the

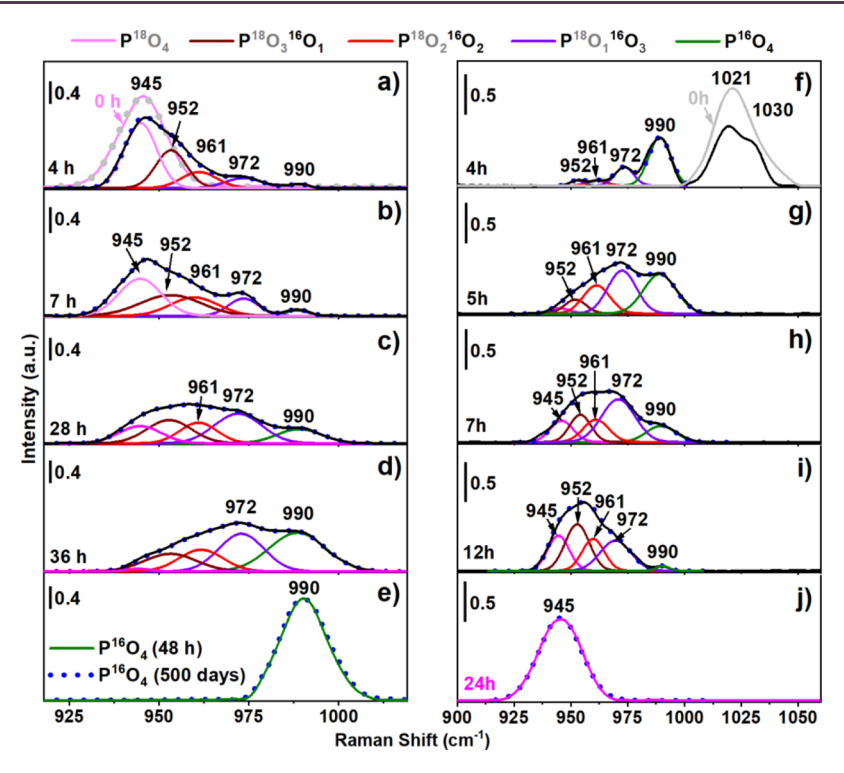


Figure 2. Raman spectra showing the kinetics of isotopologue evolution. (a–e) Isotope exchange between $P^{18}O_4$ with $H_2^{16}O$ over a period of 48 h when equilibrium is reached (data on 500 d are superimposed with a dotted blue line). (f–j) Hydrolysis of PP_i and release of P_i followed by $P^{16}O_4$ isotope exchange with $H_2^{18}O$. Both columns show the 0 h data (Figure 1) overlaid in 4 h time for comparison. The evolution of isotopologues is demonstrated more clearly in the fitted spectra, which resolve various ^{18}O and ^{16}O components of each individual isotopologue over time.

 $\nu_{\rm sym}({\rm P^{18}O_2^{16}O_2}),~\nu_{\rm sym}({\rm P^{18}O^{16}O_3}),~\nu_{\rm sym}({\rm ^{18}O^{16}O_3}),~{\rm and}~\nu_{\rm sym}({\rm ^{16}O_4})$ was corrected to follow the isotope intensity sum rule but it did not make a significant difference in the proportion of computed isotopologue.

Integration of ^{31}P NMR peaks for accurate quantitation could be incorrect because of an uneven nuclear Overhauser effect (NOE) arising from broad-band decoupling. The NOE, however, can be minimized by reducing the acquisition time. Nonetheless, the difference in chemical shifts between $P^{18}O_4$ and $P^{16}O_4$ isotopologues was found to be constant (0.08 \pm 0.01 ppm) for the ranges of pH (6.0 to 10.0) analyzed. In our experiments, pH was kept constant (at 9.0 \pm 0.1), and the solution chemistry was essentially the same. Because any apparent changes in chemical shifts in samples collected at different time points were not observed, the impact of NOE to influence the isotopologue mass calculation is expected to be insignificant.

■ RESULTS AND DISCUSSION

Characterization of ^{16}O - and ^{18}O -Labeled P_i and PP_i Using Raman and NMR Spectroscopy Methods. The Raman spectrum of 99.7% $P^{18}\text{O}_4$ at pH 9.0 generated three distinct bands at 810, 945, and 1039 cm $^{-1}$ (Figure 1a). The two bands at 810 and 945 cm $^{-1}$ are responsible for the symmetrical stretching (ν_{sym}) band of P_{ij} the band at 1039 cm $^{-1}$ represents an antisymmetrical stretching (ν_{asym}) band. Similarly, the Raman spectrum for $P^{16}\text{O}_4$ has three stretching modes, slightly blue-shifted, at 875, 990, and 1080 cm $^{-1}$ (Figure 1a). The symmetric bands at 945 cm $^{-1}$ for $P^{18}\text{O}_4$ and 990 cm $^{-1}$ for $P^{16}\text{O}_4$ showed the highest intensities without any additional bands in between these two peaks (Figure 1a). Therefore, the peaks at 945 and 990 cm $^{-1}$ were chosen to monitor the evolution of quantifiable isotopologues between

two end-members, $P^{18}O_4$ and $P^{16}O_4$, respectively. The Raman spectrum of $P_2^{16}O_7$ produced a single band for the P-O-P bond at 1021 cm⁻¹ (Figure 1b), which is distinct from both $P^{18}O_4$ and $P^{16}O_4$ peaks. Furthermore, no additional bands were present for $P_2^{16}O_7$ (Figure 1b). Analogous to the Raman spectra, ^{31}P NMR spectra of $P^{18}O_4$, $P^{16}O_4$, and $P_2^{16}O_7$ each produced distinct singlet peaks at the chemical shifts of 2.62, 2.54, and -6.25 ppm, respectively (Figure 1c). The peak separation of 0.08 ppm between $P^{18}O_4$ and $P^{16}O_4$ was constant even if the pH changed, which provided an adequate peak separation to monitor the formation and disappearance of P_i isotopologues (Figure 1c).

Control experiments performed without enzymes revealed that the peak position for $P^{18}O_4$ and $P_2^{16}O_7$ remained constant during the analytical timeframe of 500 d (Figure S2), which indicated the absence of abiotic oxygen isotope exchange. Given that the isotope values between the start and end of P_{i^-} water or PP_{i^-} water systems were five to eight orders of magnitude different in enzyme-catalyzed reactions, 32 any slightest changes that occurred would have been readily noticed. Furthermore, control experiments performed with enzymes for $P^{18}O_4$ and $P_2^{16}O_7$ without the presence of the cofactor showed no enzymatic activity. While trace metal contamination in commercial enzymes is sometimes sufficient to serve as a cofactor in the enzyme-catalyzed reaction, spiking the sample solution with a cofactor was found to be required for the specific enzyme used in this study.

Enzyme-Catalyzed Phosphate-Water ($P^{18}O_4-H_2^{16}O$) Isotope Exchange. We analyzed the evolution of isotopologues during the oxygen isotope exchange between $P^{18}O_4$ and $H_2^{16}O$ using both Raman and NMR spectroscopy methods (Figure 2). The two sets of spectroscopic data are discussed in detail below.

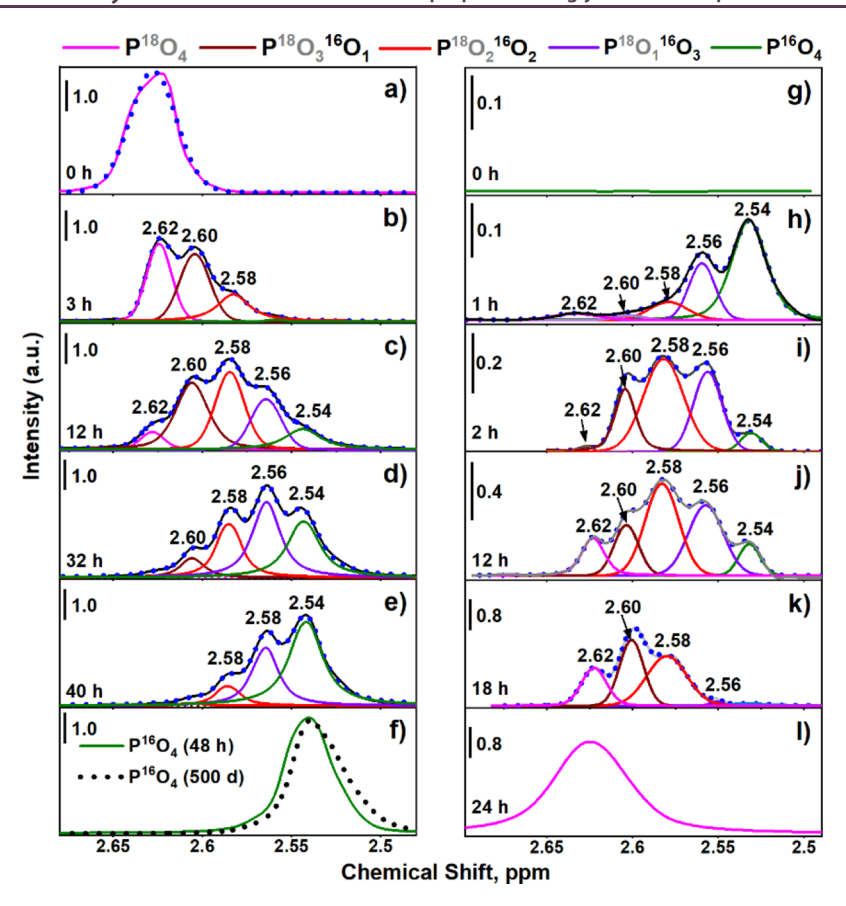


Figure 3. ^{31}P NMR spectra of oxygen isotope exchange. (a–f) Exchange between $P^{18}O_4$ and $H_2^{16}O$ and the evolution of five isotopologues over time. At 48 h, all oxygens in $P^{18}O_4$ have fully exchanged with $H_2^{16}O$. The slight shift in NMR upfield of 48 h was due to the changes in pH. (g–l) Hydrolysis of PP_i and release of P_i followed by progressive isotope exchange with water. The absence of peaks in (g) is due to different chemical shifts of PP_i out the range in the x-axis presented (see Figure 5).

Raman Spectra. A series of spectra collected over an analytical timeframe (0-48 h) during the PPase-catalyzed isotope exchange reaction showed the progressive formation of different isotopologues of P_i ($P^{18}O_4$, $P^{\tilde{18}}O_3^{16}O$, $P^{18}O_2^{16}O_2$, $P^{18}O^{16}O_3$, and $P^{16}O_4$) (Figure 2a-e). The 945 cm⁻¹ peak of P18O4 gradually diminished over time accompanied by the corresponding increase in the intensity of the P¹⁶O₄ peak at 990 cm⁻¹ (Figure 2a). To monitor the evolution of each isotopologue (Figure 2a-e), the deconvolution of experimental spectra into five different isotopologues was performed based on the observed frequencies and calculations made from the P-O bond as a harmonic oscillator (Tables S1 and S2). For example, P¹⁸O₃¹⁶O (952 cm⁻¹) became the second strongest signal at 4 h, followed by progressive increasing appearance of P18O216O2 (961 cm-1) and P18O16O3 (972 cm⁻¹), whereby P¹⁸O¹⁶O₃ eventually was the strongest peak at 28 h of reaction time (Figure 2c). The integrated intensity of each isotopologue at different time points shows that the P¹⁸O₃¹⁶O₁ and P¹⁸O₂¹⁶O₂ species remained relatively constant until about 36 h (Figure 2d). A comparison of slopes of the integrated intensity of each isotopologue revealed the steadystate concentration (i.e., formation minus transformation into other isotopologues was constant) of these two isotopologues (Figure S1). The slopes of P18O4 and P16O4, the end member isotopologues, were the same magnitude but of opposite sign (Figure S1). After 48 h, no significant change was found in the spectra for up to 500 d of the experiment (Figure 2e). It is also worth noting that at time 0 h there is no visibly distinguishable

peak for $P^{16}O_4$ (Figure 2a), which consisted of 0.3% of the total area originated from ^{16}O present in the $P^{18}O_4$ system. Similarly, data on 48 h and 500 d showed no visibly distinguishable peaks for $P^{18}O_4$, which consisted of 0.2% of the total area (Figure 2e).

NMR Spectra. We also quantified the kinetics of isotope exchange of each isotopologue in ³¹P NMR as the P¹⁸O₄ continued to exchange with H₂ ¹⁶O for 48 h (Figure 3a-f). The ³¹P NMR data generally concurred with the Raman data, albeit with some minor differences (Figures 2 and 3). As the P¹⁸O₄ was progressively substituted, P18O316O, P18O216O2, P18O116O3, and P16O4 isotopologue peaks gradually appeared whereby the peaks for lighter mass isotopologues became relatively more intense over time (Figure 3a-f). For example, P¹⁸O₂¹⁶O₂ (2.58 ppm) became the strongest signal at 12 h of reaction time, whereas $P^{18}O_1^{16}O_3$ (2.56 ppm) and $P^{16}O_4$ (2.54 ppm) peaks became predominant at 32 h and 40 h, respectively (Figure 3c-f). The 2.62 ppm peak area of P¹⁸O₄ steadily decreased and eventually almost disappeared by 48 h, at which time the signal for isotopologue P16O4 at 2.54 ppm reached its maximum intensity (Figure 3f). After 48 h, no significant changes occurred in the ³¹P NMR spectra up to 500 d (Figure 3f). The slight upfield shift in 500 d is caused by the small change in the pH which may have been due to a small amount of evaporation. Our data agreed with previously published Raman and ³¹P NMR spectra. ^{25,28} Further, it provided high-resolution time-resolved kinetics of each

isotopologue, which was cross-validated by independent NMR and Raman spectroscopy methods.

Kinetics of the Oxygen Isotope Exchange between Phosphate and Water. The calculated isotopic values based on the measured integrated intensities for Raman and NMR spectra can be used to determine the overall kinetics of isotope exchange. The overall exchange of oxygen isotopes between $P^{18}O_4$ and $H_2^{16}O$ can be expressed as:

$$[P^{18}O_4]^{3-} + 4[H_2^{O}] \overset{k}{\underset{k'}{\rightleftharpoons}} [P^{16}O_4]^{3-} + 4[H_2^{O}]$$

where k and k' are the overall rate constants of the forward and reverse reactions (s⁻¹), respectively. Isotope exchange reactions are first-order rate reactions. ^{33,34} Raman and NMR spectroscopy data show linear trends that are parallel to one another confirming that oxygen isotope exchange between P¹⁸O₄ and H₂¹⁶O is a first-order rate reaction $[-\ln(1-f)]$ vs time in Figure S2]. The slope of the linear regression was used to determine the overall rate of the exchange reaction, which was 3.33×10^{-6} s⁻¹ ($\pm 4.61 \times 10^{-5}$) and 3.43×10^{-6} s⁻¹ ($\pm 8.83 \times 10^{-5}$) for Raman and NMR, respectively. Similar rate constants in Raman and NMR (p-values < 0.05), indicate that these methods could be used interchangeably for quantifying isotope exchange reactions.

We calculated the oxygen isotope exchange between P¹⁸O₄ and water, from the measured peak area of integration for the two end-member phosphate oxygen isotopologues (Figure 4).

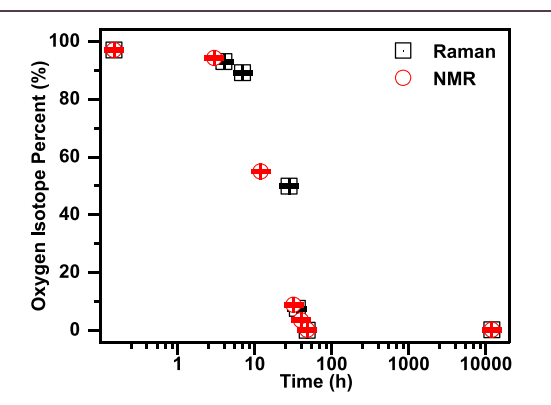


Figure 4. Isotope exchange expressed as the percent of ^{18}O remining over time. Data were calculated from area integration of the two isotopologues ($P^{18}\text{O}_4$ and $P^{16}\text{O}_4)$ as a function of time in Raman and NMR spectra.

This method allowed quantifying the lowest concentration of ¹⁸O that can be readily detected by Raman and NMR. For accurate calculation of isotope values using this method, a higher concentration of ¹⁸O is required (Figure S3). The final oxygen isotope ratios calculated from Raman and NMR were found to be in agreement with one another (Figure 4), implying that calculation of isotope abundance of each isotopologue as fractions of the total intensity without isotope mass correction did not contribute any significant error.

The P¹⁸O₄ peak intensity rapidly decreased first and gradually approached a steady-state (Figures 2a–e and 3a–f). For instance, after 48 h of reaction time, the peak intensities in both Raman and NMR spectra had little to no observable changes (Figures 2e and 3f). Spectra collected at much longer incubation time, 96 h and 500 d, was not different from 48 h, which confirmed that the equilibrium state was achieved around 48 h time. We found that the parameters of the linear

regressions in this study are within reasonable agreement with past studies (PPase-catalyzed exchange reaction). 1,25,35,36 Furthermore, PPase used in this study was from *E. coli*, whereas past studies 1,25,35,36 were from different yeast sources. The similarity in rate constants implied that the enzyme kinetics is independant of at least these two sources specificity of enzymes.

Enzyme-Catalyzed Pyrophosphate-Water (P₂¹⁶O₇ in H₂¹⁸O) Isotope Exchange. Both the hydrolysis of PP_i and subsequent oxygen isotope exchange reaction of P_i with water are catalyzed by PPase. We found that both reactions were clearly distinct and separable in Raman and NMR data (Figures 2 and 3).

Raman Spectra. The rapid hydrolysis of PP_i was apparent from the decrease in the Raman peak at 1021 cm⁻¹, which disappeared after 5 h (Figure 2f). Loss of the PP, signal was accompanied by the subsequent appearance of several Pi isotopologues (Figure 2f). By 4 h of reaction, a shoulder appeared at 1030 cm⁻¹ in the Raman spectra which was not apparent in earlier time spectra. This shoulder may have originated from Fermi resonance because of wavefunction mixing by shifting energies.³⁷ The formation of five P_i isotopologues (P¹⁸O₄, P¹⁸O₃¹⁶O, P¹⁸O₂¹⁶O₂, P¹⁸O¹⁶O₃, and P¹⁶O₄) was similar to the P_i-water exchange reaction (Figure 2a-e) but toward lower wavenumbers due to progressive exchange of ¹⁶O in P_i by ¹⁸O in water (as opposed to ¹⁸O in P_i by ¹⁶O in water in Figure 2a-e). By 24 h, the P¹⁸O₄ peak at 945 cm⁻¹ was found to be the only dominant peak with no significant changes occurring thereafter until 500 d of incubation (Figure 2j).

NMR Spectra. The ^{31}P NMR data validated the formation of five P_i isotopologues, analogous to Raman data (Figure 3g–l). When comparing the NMR spectra to the Raman spectra at and after 4 h, no abnormal peaks appeared, further validating the existence of Fermi resonance in the Raman spectra at a time point when hydrolysis and condensation reactions occurred simultaneously (Figure 2f). This result is consistent with the base-catalyzed hydrolytic reaction in PP_i as a concerted SN2-type reaction with simultaneous formation and breakage of the P–O bonds. As expected, the order of formation of heavier isotopologues at the expense of lighter isotopologues in the $P_2^{16}O_7$ and $P_2^{18}O$ (i.e., P_i derived from PP_i) was inverse to that of the $P_1^{18}O_4$ and $P_2^{16}O_5$ system (Figure 3a–f).

Comparing the kinetics of formation of isotopologues in the $P^{16}O_4$ and $H_2^{18}O$ system vs the $P^{18}O_4$ and $H_2^{16}O$ system, the former had a higher reaction rate (nearly one-half of the time) that resulted in the complete oxygen isotope exchange of P_i in 24 h (compare Figures 2a-e vs f-j and 3a-f vs g-l). This result is attributed to the higher concentration of Mg²⁺ (50 vs 5 mM in first and second systems, respectively), which facilitates the formation of the Mg-P_i complex that binds to active sites in the enzyme, a prerequisite for the formation of PP, 38 The difference in the concentration of the metal cofactor did not affect the oxygen isotope exchange because the reversible hydrolysis-condensation reaction continues as long as the enzyme is active. However, the difference in concentration changed the reaction kinetics, which is useful for manipulation of reaction rates to accommodate the spectral resolution time needed in different analytical methods.

A noteworthy finding in this study was that, when PP_i was present at a high concentration, the hydrolysis reaction dominated and the PP_i appeared to be eliminated by 24 h of

reaction (Figure 5). It was reported that the steady-state concentration of PP_i in the hydrolysis—condensation reactions

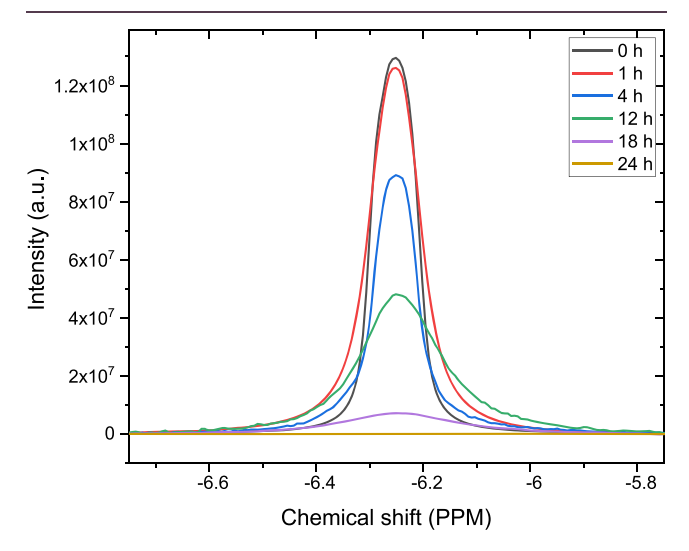


Figure 5. 31 P NMR spectra showing the decrease in PP_i concentration over time. The apparent absence of peaks in 24 h is due to the choice of scale. The remaining concentration of PP_i on and after 24 h was \sim 0.3 mM.

would be quite low (around 10 μ M when concentrations of P_i and Mg^{2+} are 50 and 20 mM, respectively³⁹). This steady-state PP_i concentration would be below the limits of detection for the NMR method (~2 mM). Aside from PP_i and isotopologues of P_i , no other peaks were found in Raman or NMR spectra (Figures 2 and 3).

Future Perspectives on Phosphate Oxygen Isotopologues. The equilibrium thermodynamic effect is one of the many mechanisms of isotopic fractionation that leads to the distinctive proportions of different isotopologues. On the other hand, a nonequilibrium process is considered the major reason for multiple interpretations under the implicit assumptions that equilibrium exchange would be achieved. Therefore, the realistic interpretation of environmental processes based on the isotope data relies on the knowledge of the kinetics of isotope exchange between different interacting aqueous species. Information on kinetics aids in identifying whether reaction time was sufficient for the complete equilibration of the P_i species before incorporation into minerals, in which isotope values are faithfully preserved.

The major limitation of applying current P, oxygen isotope thermometry 43,44 in the deep past or extant ecosystem is the inability to collect coexisting ambient water, in which P_i is equilibrated, for isotopic measurements. Earlier work on isotope effects in irreversible reactions constrained site-specific isotope analysis, 45 as is the case for P_i present in more than one structural position. The data presented in this study provide a way forward for the development of a tool in determining isotope percentages and the potential for isotopic fractionation calculations among different isotopologues or the same isotopologue present in different sites in a molecule, which might have different rates of isotope exchange. The interrelationship among isotopologues at various sites in a molecule may circumvent the need to analyze coexisting water at the time of mineral formation and thus provide a basis of fractionation among them as potential new isotope thermometry. If successful, they can be used to reconstruct pore water oxygen isotope compositions in past environments as well as modern terrestrial environments like soils where the oxygen isotope pore water varies significantly in both space and time.

ASSOCIATED CONTENT

5 Supporting Information

The Supporting Information is available free of charge at https://pubs.acs.org/doi/10.1021/acsearthspace-chem.2c00050.

Theoretical and measured Raman shift positions of phosphate isotopologues (Table S1, S2), changes in intensities of isotopologues during oxygen isotope exchange (Figure S1), rate of the isotope exchange reaction (Figure S2), and peak fitting of measured data (Figure S3) (PDF)

AUTHOR INFORMATION

Corresponding Author

Deb P. Jaisi – Department of Plant and Soil Sciences, University of Delaware, Newark, Delaware 19716, United States; ⊕ orcid.org/0000-0001-8934-3832; Phone: (302) 831-1376; Email: jaisi@udel.edu

Authors

Spencer R. Moller – Department of Plant and Soil Sciences, University of Delaware, Newark, Delaware 19716, United States; orcid.org/0000-0003-1423-0563

Yuriy Sakhno – Department of Plant and Soil Sciences, University of Delaware, Newark, Delaware 19716, United States

Ludmilla Aristilde — Department of Civil and Environmental Engineering, Northwestern University, Evanston, Illinois 60208, United States; orcid.org/0000-0002-8566-1486

Ruth E. Blake – Department of Geology and Geophysics, Yale University, New Haven, Connecticut 04520, United States

Complete contact information is available at: https://pubs.acs.org/10.1021/acsearthspacechem.2c00050

Notes

The authors declare no competing financial interest.

ACKNOWLEDGMENTS

This research was supported by a collaborative grant from the U.S. National Science Foundation awarded to DJ and LA (CHE-1709724 and CHE-1709626, respectively) and a Fellowship to SM from the Delaware Environmental Institute. Mention of trade names or commercial products in this publication is solely for the purpose of providing specific information and does not imply recommendation or endorsement by the National Science Foundation.

REFERENCES

- (1) Blake, R. E.; O'Neil, J. R.; Surkov, A. V. Biogeochemical cycling of phosphorus: Insights from oxygen isotope effects of phosphoenzymes. *Am. J. Sci.* **2005**, 305, 596–620.
- (2) Stout, L. M.; Joshi, S. R.; Kana, T. M.; Jaisi, D. P. Microbial activities and phosphorus cycling: An application of oxygen isotope ratios in phosphate. *Geochim. Cosmochim. Acta* **2014**, *138*, 101–116.
- (3) Helfenstein, J.; Tamburini, F.; von Sperber, C.; Massey, M. S.; Pistocchi, C.; Chadwick, O. A.; Vitousek, P. M.; Kretzschmar, R.; Frossard, E. Combining spectroscopic and isotopic techniques gives a

- dynamic view of phosphorus cycling in soil. Nat. Commun. 2018, 9, 3226.
- (4) Cohn, M. Phosphate-water exchange reaction catalyzed by inorganic pyrophosphatase of yeast. *J. Biol. Chem.* **1958**, 230, 369–379
- (5) Knowles, J. R. Enzyme-catalyzed phosphoryl transfer reactions. *Annu. Rev. Biochem.* **1980**, *49*, 877–919.
- (6) Heikinheimo, P.; Lehtonen, J.; Baykov, A.; Lahti, R.; Cooperman, B. S.; Goldman, A. The structural basis for pyrophosphatase catalysis. *Structure* **1996**, *4*, 1491–1508.
- (7) Chen, J.; Brevet, A.; Fromant, M.; Leveque, F.; Schmitter, J.; Blanquet, S.; Plateau, P. Pyrophosphatase is essential for growth of *Escherichia coli. J. Bacteriol.* **1990**, *172*, 5686–5689.
- (8) Harvey, G. W.; Keister, D. L. Energy-linked reactions in photosynthetic bacteria pi reversible hoh oxygen-exchange catalyzed by the membrane-bound inorganic pyrophosphatase of *rhodospirillum-rubrum* .11. *Arch. Biochem. Biophys.* **1981**, 208, 426—430.
- (9) Baykov, A. A.; Shestakov, A. S.; Kasho, V. N.; Vener, A. V.; Ivanov, A. H. Kinetics and thermodynamics of catalysis by the inorganic pyrophosphatase of *Escherichia coli* in both directions. *Eur. J. Biochem.* **1990**, *194*, 879–887.
- (10) Kornberg, A. Pyrophosphorylases and phosphorylases in biosynthetic reactions. *Adv. Enzymol. Related Areas Mol. Biol.* **1957**, 18, 191–240.
- (11) Kottur, J.; Nair, D. T. Pyrophosphate hydrolysis is an intrinsic and critical step of the DNA synthesis reaction. *Nucleic Acids Res.* **2018**, *46*, 5875–5885.
- (12) Jaisi, D. P.; Blake, R. E. Advances in using oxygen isotope ratios of phosphate to understand phosphorus cycling in the environment. In *Advances in Agronomy*; Elsevier, 2014; Vol. 125, pp 1 –53.
- (13) Jaisi, D. P.; Kukkadapu, R. K.; Stout, L. M.; Varga, T.; Blake, R. E. Biotic and abiotic pathways of phosphorus cycling in minerals and sediments: insights from oxygen isotope ratios in phosphate. *Environ. Sci. Technol.* **2011**, *45*, 6254–6261.
- (14) Liang, Y.; Blake, R. Oxygen isotope signature of Pi regeneration from organic compounds by phosphomonoesterases and photo-oxidation. *Geochim. Cosmochim. Acta* **2006**, *70*, 3957–3969.
- (15) Joshi, S. R.; Kukkadapu, R. K.; Burdige, D. J.; Bowden, M. E.; Sparks, D. L.; Jaisi, D. P. Organic matter remineralization predominates phosphorus cycling in the mid-bay sediments in the Chesapeake Bay. *Environ. Sci. Technol.* **2015**, 49, 5887–5896.
- (16) Mingus, K. A.; Liang, X. M.; Massoudieh, A.; Jaisi, D. P. Stable isotopes and bayesian modeling methods of tracking sources and differentiating bioavailable and recalcitrant phosphorus pools in suspended particulate matter. *Environ. Sci. Technol.* **2019**, *53*, 69–76.
- (17) Pistocchi, C.; Meszaros, E.; Frossard, E.; Bunemann, E. K.; Tamburini, F. In or out of equilibrium? how microbial activity controls the oxygen isotopic composition of phosphate in forest organic horizons with low and high phosphorus availability. *Front. Environ. Sci.* **2020**, *8*, No. 564778.
- (18) Urey, H. C. The thermodynamic properties of isotopic substances. J. Chem. Soc. 1947, 562-581.
- (19) Geisler, T.; Perdikouri, C.; Kasioptas, A.; Dietzel, M. Real-time monitoring of the overall exchange of oxygen isotopes between aqueous ${\rm CO_3}^{2-}$ and ${\rm H_2O}$ by Raman spectroscopy. *Geochim. Cosmochim. Acta* **2012**, *90*, 1–11.
- (20) Zeebe, R. E. A new value for the stable oxygen isotope fractionation between dissolved sulfate ion and water. *Geochim. Cosmochim. Acta* **2010**, *74*, 818–828.
- (21) Antler, G.; Turchyn, A. V.; Rennie, V.; Herut, B.; Sivan, O. Coupled sulfur and oxygen isotope insight into bacterial sulfate reduction in the natural environment. *Geochim. Cosmochim. Acta* **2013**, *118*, 98–117.
- (22) Bertran, E.; Waldeck, A.; Wing, B.; Halevy, I.; Leavitt, W.; Bradley, A.; Johnston, D. Oxygen isotope effects during microbial sulfate reduction: applications to sediment cell abundances. *ISME J.* **2020**, *14*, 1508–1519.

- (23) Levitt, N. P.; Romanek, C. S. An "on-line" method for oxygen isotope exchange between gas-phase CO₂ and water. *Aquat. Geochem.* **2016**, 22, 253–269.
- (24) Zhou, T.; Wu, T.; Wu, Q.; Ye, C.; Hu, R.; Chen, W.; He, X. Real-time measurement of CO_2 isotopologue ratios in exhaled breath by a hollow waveguide based mid-infrared gas sensor. *Opt. Express* **2020**, 28, 10970–10980.
- (25) von Sperber, C.; Lewandowski, H.; Tamburini, F.; Bernasconi, S. M.; Amelung, W.; Frossard, E. Kinetics of enzyme-catalysed oxygen isotope exchange between phosphate and water revealed by Raman spectroscopy. *J. Raman Spectrosc.* **2017**, *48*, 368–373.
- (26) Eiler, J. M. The isotopic anatomies of molecules and minerals. *Annu. Rev. Earth Planet. Sci.* **2013**, 41, 411–441.
- (27) Vennemann, T. W.; Fricke, H. C.; Blake, R. E.; O'Neil, J. R.; Colman, A. Oxygen isotope analysis of phosphates: a comparison of techniques for analysis of Ag₃PO₄. *Chem. Geol.* **2002**, *185*, 321–336.
- (28) Cohn, M.; Hu, A. Isotopic (¹⁸O) shift in ³¹P nuclear magnetic resonance applied to a study of enzyme-catalyzed phosphate—phosphate exchange and phosphate (oxygen)—water exchange reactions. *Proc. Natl. Acad. Sci. U. S. A.* **1978**, 75, 200–203.
- (29) Lewis, I. R.; Edwards, H. Handbook of Raman Spectroscopy: From the Research Laboratory to the Process Line; CRC Press, 2001.
- (30) Ashton, L.; Johannessen, C.; Goodacre, R. The importance of protonation in the investigation of protein phosphorylation using Raman spectroscopy and Raman optical activity. *Anal. Chem.* **2011**, 83, 7978–7983.
- (31) Liu, C.; McGovern, G. P.; Liu, P.; Zhao, H.; Horita, J. Position-specific carbon and hydrogen isotopic compositions of propane from natural gases with quantitative NMR. *Chem. Geol.* **2018**, *491*, 14–26.
- (32) McKay, H. Kinetics of exchange reactions. *Nature* **1938**, 142, 997–998.
- (33) Kasioptas, A.; Geisler, T.; Perdikouri, C.; Trepmann, C.; Gussone, N.; Putnis, A. Polycrystalline apatite synthesized by hydrothermal replacement of calcium carbonates. *Geochim. Cosmochim. Acta* **2011**, *75*, 3486–3500.
- (34) Chang, S. J.; Blake, R. E.; Colman, A. S. Oxygen isotope exchange rates between phosphate and water catalyzed by inorganic pyrophosphatase: Implications for the biogeochemical cycle of phosphorus. *Earth Planet. Sci. Lett.* **2021**, *570*, No. 117071.
- (35) Blake, R. E.; O'neil, J.; Garcia, G. A. Oxygen isotope systematics of biologically mediated reactions of phosphate: I. Microbial degradation of organophosphorus compounds. *Geochim. Cosmochim. Acta* 1997, 61, 4411–4422.
- (36) Chang, S. J.; Blake, R. E. Precise calibration of equilibrium oxygen isotope fractionations between dissolved phosphate and water from 3 to 37 C. *Geochim. Cosmochim. Acta* **2015**, *150*, 314–329.
- (37) Amat, G.; Pimbert, M. On Fermi resonance in carbon dioxide. *J. Mol. Spectrosc.* **1965**, *16*, 278–290.
- (38) Smirnova, I. N.; Kasho, V. N.; Volk, S. E.; Ivanov, A. H.; Baykov, A. A. Rates of elementary steps catalyzed by rat-liver cytosolic and mitochondrial inorganic pyrophosphatases in both directions. *Arch. Biochem. Biophys.* **1995**, *318*, 340–348.
- (39) Baykov, A. A.; Shestakov, A. S. Pathways of pyrophosphate hydrolysis and synthesis by yeast inorganic pyrophosphatase. *Eur. J. Biochem.* **1992**, *206*, 463–470.
- (40) Eiler, J. M. The isotopic anatomies of molecules and minerals. In *Annual Review of Earth and Planetary Sciences*, Jeanloz, R., Ed.; California Institute of Technology, Pasadena, California, 2013; Vol. 41, pp 411–441.
- (41) Blake, R. E.; Chang, S. J.; Lepland, A. Phosphate oxygen isotopic evidence for a temperate and biologically active Archaean ocean. *Nature* **2010**, *464*, 1029–1032.
- (42) Jaisi, D. P.; Blake, R. E. Tracing sources and cycling of phosphorus in Peru Margin sediments using oxygen isotopes in authigenic and detrital phosphates. *Geochim. Cosmochim. Acta* **2010**, 74, 3199–3212.
- (43) Chang, S. J.; Blake, R. E. Precise calibration of equilibrium oxygen isotope fractionations between dissolved phosphate and water

from 3 to 37 degrees C. Geochim. Cosmochim. Acta **2015**, 150, 314–329.

- (44) Longinelli, A.; Nuti, S. Revised phosphate-water isotopic temperature scale. *Earth Planet. Sci. Lett.* **1973**, *19*, 373–376.
- $(4\hat{s})$ Singleton, D. A.; Thomas, A. A. High-precision simultaneous determination of multiple small kinetic isotope effects at natural abundance. *J. Am. Chem. Soc.* **1995**, 117, 9357–9358.